Supplementary information for "A magnetically-induced Coulomb gap in graphene due to electron-electron interactions"

Evgenii E. Vdovin,[1,2] Mark T. Greenaway,[3] Yurii N. Khanin,[2] Sergey V. Morozov,[2] Oleg Makarovsky,[1] Amalia Patanè,[1] Artem Mishchenko,[4,5] Sergey Slizovskiy,[4,5] Vladimir Fal'ko,[4,5,6] Andre K. Geim,[4,5] Kostya S. Novoselov,[7] and Laurence Eaves[1]

[1] *School of Physics and Astronomy, University of Nottingham, Nottingham, NG7 2RD, UK*
[2] *Institute of Microelectronics Technology RAS, Chernogolovka 142432, Russia*
[3] *Department of Physics, Loughborough University, Loughborough, LE11 3TU, UK*
[4] *Department of Physics and Astronomy, University of Manchester, Manchester, M13 9PL, UK*
[5] *National Graphene Institute, University of Manchester, Manchester, M13 9PL, UK*
[6] *Henry Royce Institute for Advanced Materials, University of Manchester, Manchester, M13 9PL, UK*
[7] *Institute for Functional Intelligent Materials, National University of Singapore, 4 Science Drive 2, Singapore 117544.*
(Dated: June 14, 2023)

Supplementary Note 1: Electrostatic model

We analysed the electrostatic properties of our tunnel transistors using a parallel-plate capacitor model [1–3]. The model includes the effect of the low density of states in graphene that only partially screens the gate electric field. We obtain the following simultaneous equations:

$$eV_{\mathrm{b}} = \mu_{\mathrm{B}} - \mu_{\mathrm{T}} - \Delta E_{\mathrm{D}}, \tag{S1}$$

$$eV_{\mathrm{g}} = \mu_{\mathrm{B}} + \frac{e^2 D_{\mathrm{g}}(n_{\mathrm{T}} + n_{\mathrm{B}})}{\varepsilon_{\mathrm{s}}\varepsilon_0}, \tag{S2}$$

where $\mu_{\mathrm{B,T}}$ and $n_{\mathrm{B,T}}$ are the chemical potentials and carrier densities on the bottom ($\mathrm{Gr_B}$) and top ($\mathrm{Gr_T}$) graphene layers, respectively, $D_{\mathrm{g}} = 26$ nm is the hBN substrate thickness, $\varepsilon_{\mathrm{s}} = 3.2$ is the relative permittivity of the hBN substrate, and v_{F} is the Fermi velocity in graphene. ΔE_{D} is the energy band offset between the Dirac points top and bottom layers and is given by

$$\Delta E_{\mathrm{D}} = eF_{\mathrm{b}}d = \frac{e^2 d n_{\mathrm{T}}}{\varepsilon_{\mathrm{s}}\varepsilon_0}, \tag{S3}$$

where F_{b} is the electric field in the barrier layer.

In a quantising magnetic field, B, and neglecting the many-body effects discussed in the main text, the density of states is transformed into a set of peaks centred on the Landau level (LL) energies $E_N = \hbar\sqrt{2N}v_{\mathrm{F}}/l_{\mathrm{B}}$, where N is the LL index, and $l_{\mathrm{B}} = \sqrt{\hbar/eB}$ is the magnetic length. We model the density of states, $A(E)$, using a set of Gaussian functions [2] which ensures convergence at low magnetic fields:

$$A(E) = \frac{2}{\pi l_{\mathrm{B}}^2\sqrt{2\pi}\Gamma}\sum_{N=-\infty}^{\infty}\exp\left(-\frac{(E-E_N)^2}{2\Gamma^2}\right). \tag{S4}$$

We neglect the N-dependent broadening of the LLs. The relation between n and μ is given by $n = \int_0^\infty A(E)f(E,\mu)dE$ where $f(E,\mu)$ is the Fermi-Dirac distribution function. At low temperatures an approximate formula is given by $n = \int_0^\mu A(E)dE$. These equations are solved self-consistently to find the electrostatic configuration for a given V_{b} and V_{g}.

To model the tunnel current through the barrier, we use the Landauer-Büttiker approach described in [3] where the current through the defect can be shown to be

$$I \propto \int (f_{\mathrm{B}} - f_{\mathrm{T}})A(E)A_{\mathrm{imp}}(E - \Delta E_{\mathrm{D}}/2)A(E - \Delta E_{\mathrm{D}})dE, \tag{S5}$$

where $A_{\mathrm{imp}}(E) = \exp(-E^2/2\sigma_{\mathrm{i}}^2)$ is the broadened spectral function of the impurity state with width σ_{i} at the centre of the barrier, and $f_{\mathrm{B,T}}$ are the Fermi-Dirac distributions in the bottom and top graphene layers, respectively.

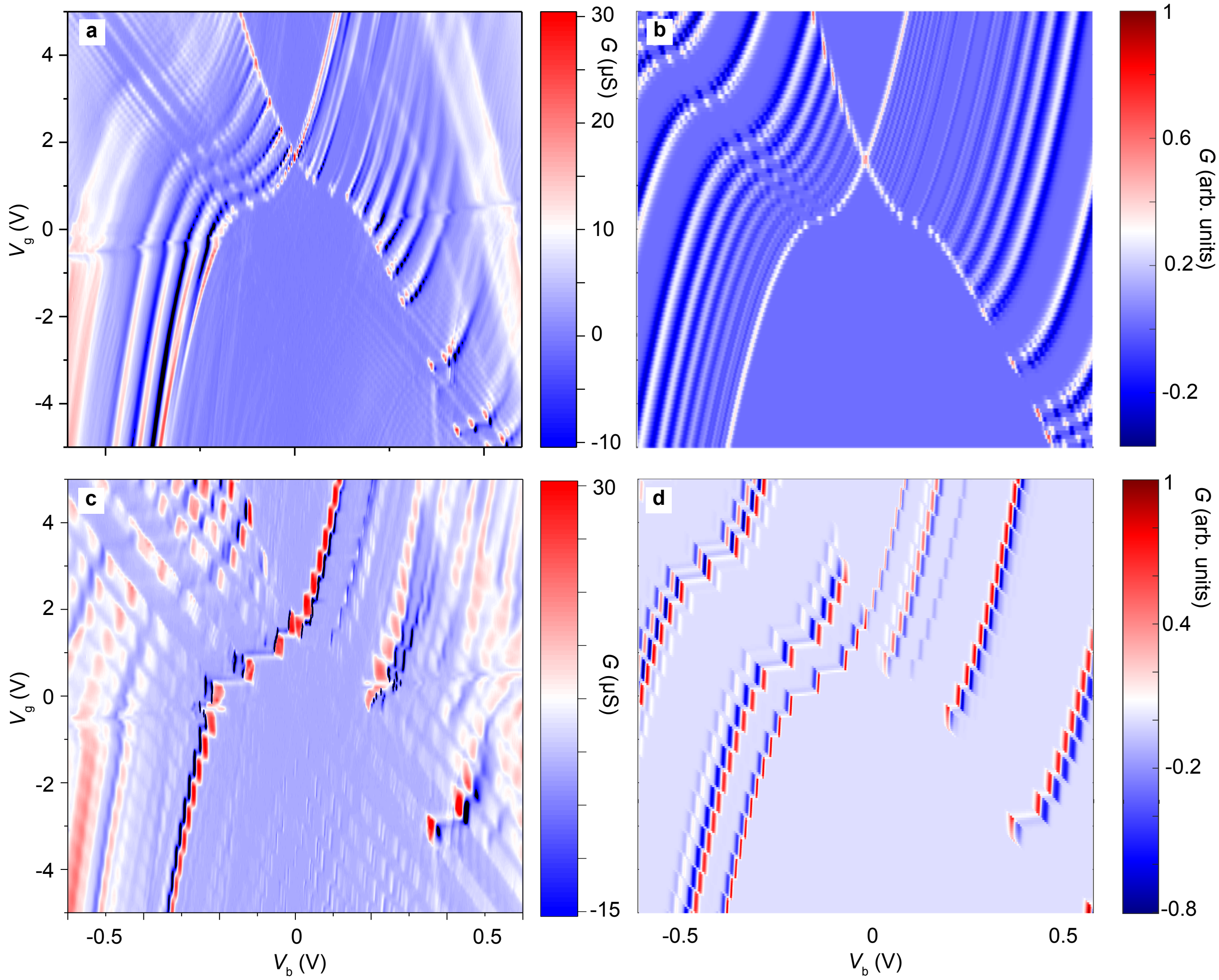

Supplementary Figure 1. Colour maps of the differential conductance $G(V_g, V_b)$ at $T = 1.6$ K and $B = 1$ T (panels **a** and **b**) and $B = 4$ T (panels **c** and **d**). Panels **a** and **c** are the measured maps and panels **b** and **d** were calculated using the model presented in Supplementary Note 1.

The colour maps in Supplementary Figure 1 show a comparison between the measured and modelled $G(V_g, V_b)$ maps when $B = 1$ T and 4 T. The good agreement between the maps demonstrate the validity of our electrostatic model.

Supplementary Figure 2 shows the colour map of $G(V_g, V_b)$ in a magnetic field of $B = 3.75$ T, corresponding to the plot in Fig. 2b of the main text. The panels labelled i, ii and iii show the electrostatic configuration of the device for each of the peaks in the conductance map. The schematics show the position of the chemical potential in each layer and the LL alignments, as discussed in the main text and determined using our electrostatic model.

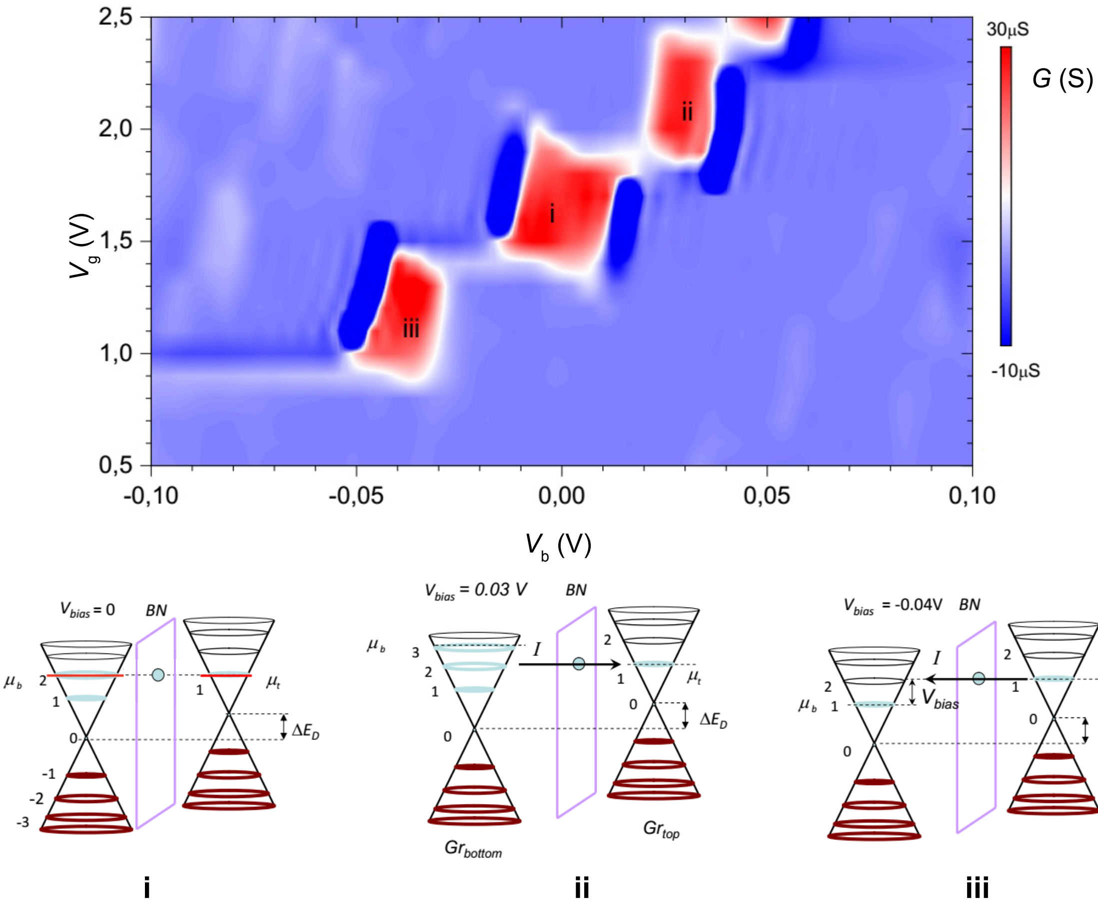

Supplementary Figure 2. Colour map of the measured $G(V_\mathrm{g}, V_\mathrm{b})$ at $B = 3.75$ T and $T = 4.2$ K, see Fig. 2b of the main text. The panels labelled i, ii and iii show the electrostatic configuration and LL alignment for the peaks in G labelled i, ii, and iii in the colour map.

Supplementary Note 2: lifting of spin and valley degeneracy

Supplementary Figure 3 shows the colour map of $G(V_\mathrm{b}, V_\mathrm{g})$ measured at $T = 0.3$ K and $B = 3.75$ T over a wider range of V_g and V_b than Fig. 2 of the main text. As discussed in the main text, the Coulomb gap emerges at low temperatures and is observed as a conductance minimum when $V_\mathrm{b} = 0$ and for $V_\mathrm{g} = 1.4$ - 1.8 V, see arrow labelled A in Supplementary Figure 3. Its bias-voltage position at $V_\mathrm{b} = 0$ is gate-voltage independent.

We also observe a different type of "splitting" of a conductance peak at low temperatures, in particular, the conductance peak labelled V-S at $V_\mathrm{g} = 0.6$ V and $V_\mathrm{b} = -0.12$ V, which is split into 4 sub-peaks due to lifting of spin- and valley degeneracy of the LLs. Our electrostatic model indicates that in this region of the plot, electrons tunnel between the $N_\mathrm{B} = 2$ and $N_\mathrm{T} = 1$ LLs, with the chemical potential in the bottom layer, μ_B, energetically aligned with the "zeroth" LL in the bottom layer, see schematic diagram inset in Supplementary Figure 3. With increasing gate voltage, the filling factor in the bottom layer varies between $\nu_\mathrm{B} = -2$ and 2 (the minus sign indicates holes). In this case, as the gate voltage is increased, the chemical potential in the bottom layer is successively pinned, and then jumps between the valley- and spin-split LLs as they are filled, giving rise to the series of four sub-peaks in the conductance. Consequently, the splittings of feature V-S have a finite slope of $\delta V_\mathrm{g}/\delta V_\mathrm{b} \approx -0.3$. We only observe this phenomena for the $N_\mathrm{B} = 0$ LL. We do not observe splitting of neighbouring conductance peaks corresponding to those with higher LL indices. The splitting of the LLs in the top graphene layer should also have a gate-voltage dependence, although we do not see evidence of splitting of the LLs in the top graphene layer in this device. Refs. [4–6] discuss the effect of spin and valley degeneracy lifting on the tunnel current in more detail. Thus, spin and valley splitting is observed in the conductance in a very different way to the minima in conductance $V_\mathrm{b} = 0$. In particular, the Coulomb gap is a gate-voltage independent feature observed as a vertical "gap" in the colour map. Therefore, we discount degeneracy lifting as an explanation for the phenomenon we ascribe to the formation of a Coulomb gap. Furthermore, we only observe the gate voltage-independent splitting of the conductance peak at $V_\mathrm{b} = 0$, which is consistent with our understanding of the mechanism of the formation of the Coulomb gap that arises due to the interaction of a low-energy tunnelling electron with the electron liquid.

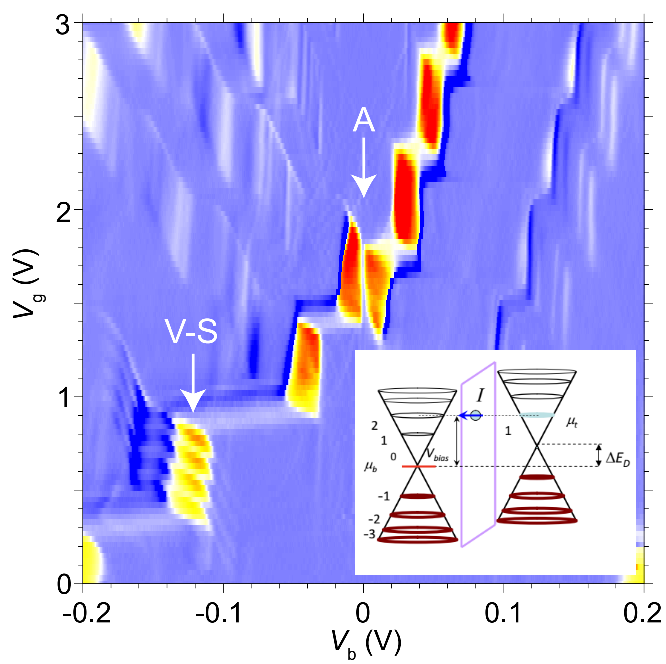

Supplementary Figure 3. Measured colour map of $G(V_\mathrm{b}, V_\mathrm{g})$ when $B = 3.75$ T and $T = 0.3$ K. Inset shows the electrostatic configuration of the device for the valley-spin "split" conductance peak labelled V-S.

SUPPLEMENTARY REFERENCES

[1] Britnell, L. et al. Field-effect tunneling transistor based on vertical graphene heterostructures. *Science* **335**, 947-950 (2012).
[2] Greenaway, M. T. et al. Resonant tunnelling between the chiral Landau states of twisted graphene lattices. *Nat. Phys.* **11**, 1057-1062 (2015).
[3] Greenaway, M. T., et al. Tunnel spectroscopy of localised electronic states in hexagonal boron nitride. *Commun. Phys.* **1**, 94 (2018).
[4] Khanin, Yu. N. et al. Observation of Spin and Valley Splitting of Landau Levels under Magnetic Tunneling in Graphene/Boron Nitride/Graphene Structures. *JETP Letters* **107**, 238 (2018).
[5] Khanin, Yu. N. et al. Tunneling in Graphene/h-BN/Graphene Heterostructures through Zero-Dimensional Levels of Defects in h-BN and Their Use as Probes to Measure the Density of States of Graphene. *JETP Letters* **109**, 482 (2019).
[6] Keren, I. et al. Quantum-dot assisted spectroscopy of degeneracy-lifted Landau levels in graphene. *Nat. Commun.* **11**, 1-9 (2020).